Chemical Papers
https://doi.org/10.1007/s11696-022-02501-9

ORIGINAL PAPER

Assessment of crystallite size of UV-synthesized hydroxyapatite using different model equations

Md. Sahadat Hossain[1] · Md. Mahfujul Hasan[1] · Monika Mahmud[1] · Mashrafi Bin Mobarak[1] · Samina Ahmed[1,2]

Received: 19 July 2022 / Accepted: 16 September 2022

Abstract

Synthesis of crystalline hydroxyapatite (Hap) commonly needs a high-temperature calcination irrespective of wet chemical or solid state synthesis protocols which eventually controls the crystallite size of Hap. Nevertheless, crystallite size of Hap is one of the top ruling parameters that restricts the reaction rate and or bone bonding ability at the artificial and natural bones interface. Concerning this fact, this present work has been designed to synthesize Hap without using any high temperature calcination but only UV-illumination of the raw materials under solid state condition. Such an effort enabled us to produce Hap successfully skipping the calcination at high temperature. Hence it was an indispensable issue to examine the effect of UV-irradiation on the crystallographic parameters particularly crystallite size (D_c) together with lattice parameters, crystallinity degree (X_c), crystallinity index (CI), dislocation density and micro-strain of Hap. Observed results disclosed that all the calculated parameters for UV-synthesized Hap are in well-matched position with those values tabulated in case of high-temperature calcination. Furthermore, we used five different models to assess the crystallite size of UV-synthesized Hap. Interestingly, among the validated five models, customary Scherrer Equation, Model of straight line passing the origin (MSLPO) in Scherrer equation and Monshi–Scherrer model provided fairly reasonable crystallite size values of 83 nm, 56 nm and 58 nm, respectively. Conversely, the crystallite size as calculated using linear straight line model (LSLM) of Scherrer's equation and Williamson–Hall (W–H) model was significantly high (723 nm and 138 nm, respectively). Such observation supports the shortcomings of these two models. However, all the observed results relating the assessment of crystallographic parameters of UV-synthesized Hap (which excluded the use of high temperature) demonstrated the compatibility of UV-method as a new synthesis route as well as the possibility of broader application of UV-Hap and this is the novelty of this work.

✉ Samina Ahmed
shanta_samina@yahoo.com

[1] Institute of Glass and Ceramic Research and Testing, Bangladesh Council of Scientific and Industrial Research (BCSIR), Dhaka 1205, Bangladesh

[2] BCSIR Dhaka Laboratories, Bangladesh Council of Scientific and Industrial Research (BCSIR), Dhaka 1205, Bangladesh

Published online: 24 September 2022

Graphical abstract

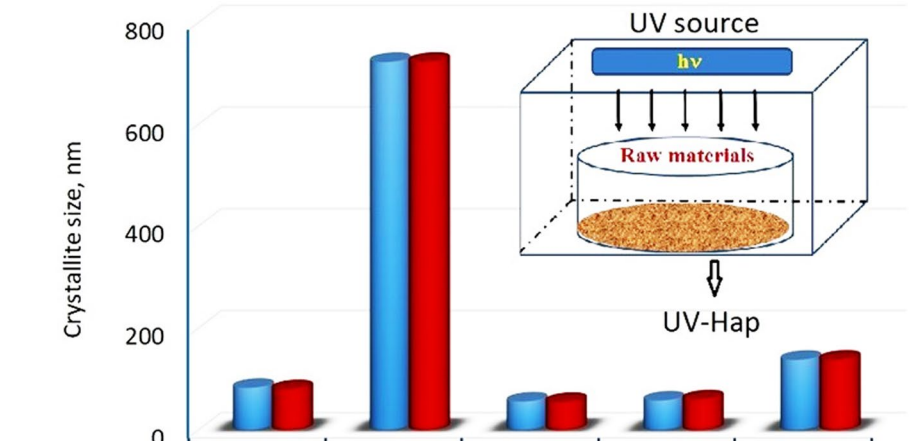

	Scherrer Eqn	LSLM of Scherrer Eqn	MSLPO in Scherrer Method	Monshi Scherrer Eqn	W - H Model
UV-Hap	83	723	56	58	138
Hap (calcined)	80	723	55	60	138

Keywords Hydroxyapatite · UV-illumination · Crystallite size · Scherrer equation · Williamson–Hall model

Introduction

Calcium hydroxyapatite (Hap) or else simply known apatite is a classic biomaterial widely used for bone tissue engineering due to its notable biocompatible, bioactive, osteoconductive and hemo-compatible characteristics. Consequently many researchers across the globe persuaded their research on Hap (Ooi et al. 2019; In et al. 2020; Becerra et al. 2022). Since various parameters, e.g., crystallite size, shape, composition and crystallinity of Hap substantially affect its application particularly in biomedical field, synthesis of Hap having dissimilar morphology has emerged as the utmost fascinating research field. In deed nowadays, to diversify the application of Hap in both healthcare and environmental fields, its synthesis using different routes and different raw materials has received ample attention. Accordingly, globally the volume of research in this arena is increasing day by day to explore its diversified applications (Hossain et al. 2022). It is being a long time that synthetic Hap is considered as an important component of bone substitution and implant fabrication (Maleki et al. 2019). The notable features of Hap which have made it a perfect candidate for biomedical applications include its ability to (1) replace bone; (2) help to regenerate or bind with surrounding tissue; (3) use as coating material for medical implants; (4) support successful implant integration, etc. (Sharifi et al. 2021). However, the application of Hap is not just restricted to bone tissue engineering/biomedical area but expanded to many more areas (e.g., drug delivery, bone grafts, adsorbents, catalysts, sensor, chromatography, etc.) as shown in Fig. 1 (Huixia et al. 2015; Maleki et al. 2019). In recent times, Hap in the form of nanoparticle has also been recommended for oral care products thus diversifying its application (Coelho et al. 2019; Sharifi et al. 2021). The ability of nano-Hap to reduce the ache related with dentin hypersensitivity promotes its application in this field. The fact is that the high surface area and considerable tiny size triggers nano-Hap to be a strong contestant in the field of biomedical research.

Crystallographically, Hap possess two types of structure: monoclinic and hexagonal while owing to considerable bioactive properties, the later type is being widely using in biomaterials industry. Hexagonal Hap consists of $P6_3/m$ space group with a sixfold symmetry axis organized with a threefold helix and a mirror plane while the standard lattice parameters are: (1) $a = b = 9.42$ Å and $c = 6.88$ Å; (2) cell volume = 530.301 $(Å)^3$; and (3) crystal density = 3.140 g cm^{-3} (Rabiei et al. 2021a, b). However, flexible structure of Hap permits ionic substitution incorporating cations with the different oxidation states but anions with the same oxidation state as OH^-, F^- or Cl^-. Such ionic substitutions are very common, which plays an important role in controlling the chemical, structural and micro-structural properties of Hap. Actually, necessary ionic substitution offers improved mechanical and physiological stabilities to Hap. In contrast, in the late 1980s, biphasic format of Hap where β-TCP exists

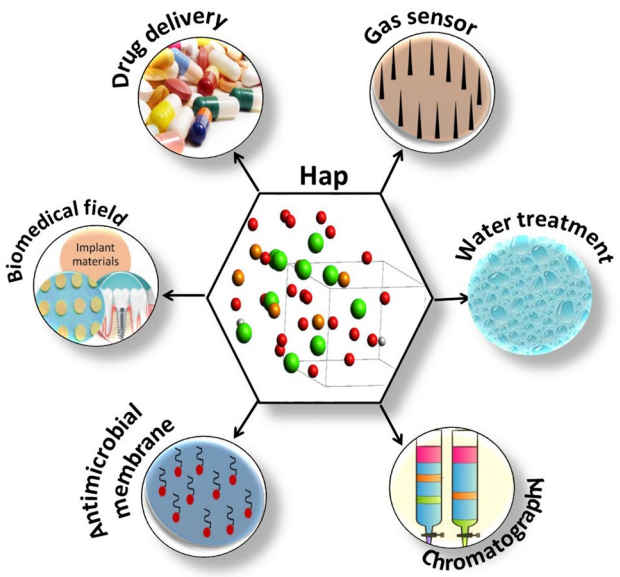

Fig. 1 Various applications of hydroxyapatite

as the 2nd phase in combination with Hap was introduced to facilitate tuned resorption criterion while needed in case of synthetic bone grafts (Gallinetti et al. 2014). However, it is well known that crystallite size of Hap is strictly depended on calcination temperature and is considered as one of the top ruling parameters. Moreover, it restricts the reaction rate at the artificial and natural bone interface. Hence, at present researchers are concerned in developing Hap through minimizing calcination temperature but with good crystallinity.

In this context, we have recently introduced UV-irradiation approach for the synthesis of Hap from eggshells where no high-temperature calcination was used (Sultana et al. 2021), and here we have addressed the effect of UV-irradiation on the crystallite size of Hap by applying different model equations.

Materials and methods

Materials

Raw eggshells as Ca-source were collected from a nearby restaurant of Science Laboratory Road, Dhanmondi, Dhaka, Bangladesh. Prior to use, the shells were thoroughly cleaned with copious amount of tap water and then boiled for 30 min. Next air drying and oven drying were accomplished at room temperature and 110 °C, respectively. Analytical grade diammonium hydrogen phosphate, $(NH_2)_4HPO_4$, was procured from E-Merck Germany. Water used for this research was deionized and prepared in the laboratory through double distillation and deionization.

Synthesis method

A very simple two step method was employed to synthesis hydroxyapatite (Hap). In the first step, maintaining Ca/P molar ratio 1.67, requisite amount of eggshell (10.52 g) and $(NH_4)_2HPO_4$ (7.90 g) was ball milled for 3 h at 550 rpm under slightly moisten condition. A high energy ball mill (Model: MSK-SFM-1 QM 3SP2) facilitated this operation. After the completion of ball mill operation, the mixture of raw materials was divided into three portions. The first and second lots were oven dried (at 110 °C) and calcined (at 900 °C), respectively. The reason behind choosing 900 °C as the optimum temperature was accredited to the decarbonization process since usually it continues up to 900 °C (Nasiri et al. 2021). The formation of Hap was examined by XRD analysis. On the other hand, the third share was irradiated by a UV-lamp of 254 nm wavelength (Model: UVLS-28 EL Series UV Lamp). However, before irradiation, the mixture was turned to paste by adding 20% DI water. A continuous illumination of 8 h transformed the raw materials into Hap according to the following reaction scheme (Eq. 1) whereas the entire synthesis procedure is depicted in Fig. 2.

$$\text{Eggshell}(CaCO_3) + (NH_4)_2HPO_4 \xrightarrow[h\upsilon]{} Ca_{10}(PO_4)_6(OH)_2 \quad (1)$$

X-ray crystallographic characterization

Phase characterization of the UV-mediated Hap was carried out using an X-ray diffractometer (Model: PANalytical X'pert PRO XRD PW 3040). Setting the scanning range at $2\theta = 5°–75°$, the data were collected in a continuous scanning mode while the scanning step was 0.01. The radiation source CuKa ($\lambda = 1.54060$) was operated at a combination of 40 kV and 30 mA, whereas cooling temperature was fixed at 19–20 °C. A parallel study was carried out using Hap sample synthesized by calcining the raw materials at 900 °C. All the observed phases were confirmed by comparing with standard JCPDS files.

Particle size analysis

Using nanoparticle analyzer (Model: Horiba Scientific, Nano Partica, SZ-100V2) equipped with a high power laser (100 mW), particle size of UV-synthesized Hap was measured employing dynamic light scattering (DLS) technology. During the course of measurement, UV-Hap powder was sonicated in water for 20 min to reduce the cluster formation and the particle sizes were determined following the method as described earlier (Anderson et al. 2013).

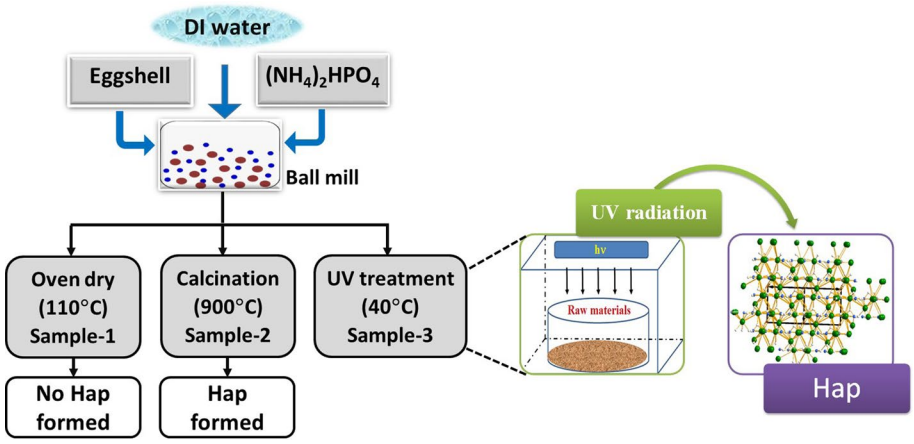

Fig. 2 Flowchart representation of Hap formation by UV-illumination of eggshell

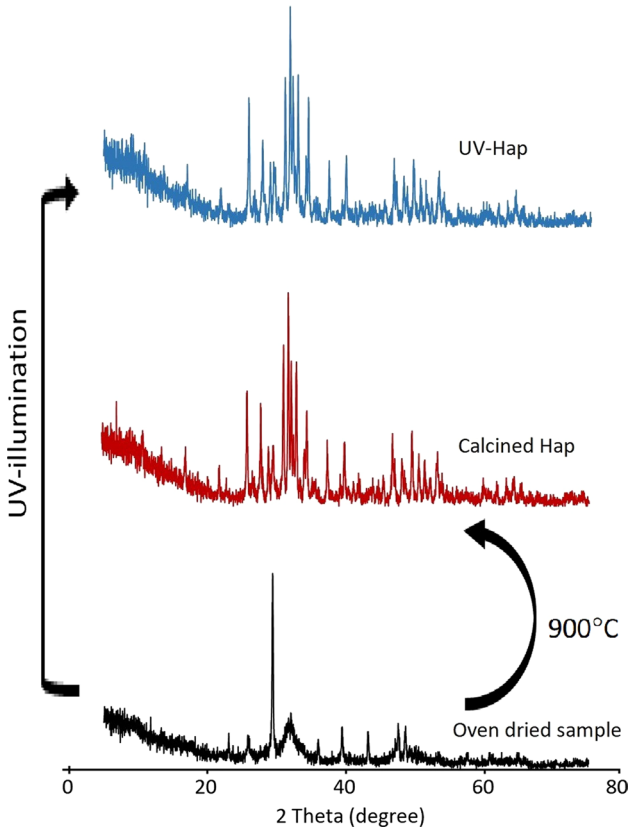

Fig. 3 X-ray diffractogram of oven dried, UV-synthesized and calcined hydroxyapatites

Results and discussion

Phase identification

The XRD patterns of UV-irradiated Hap along with the oven dried and calcined (900 °C) samples are given in Fig. 3. The diffraction peaks of the oven dried sample though visualizes a broad hump conjoining three representative peaks for Hap at 211, 112 and 300 planes but the strong diffraction peak at 29.41° position (104 plane) carries good evidence regarding the presence of $CaCO_3$ as the leading phase. Such evidence supports that only oven drying of the raw materials is not enough to complete the reaction to form hydroxyapatite. On the other hand, calcination of the starting materials at 900 °C gives high intensity peaks corresponding to hydroxyapatite (Fig. 3). The major peaks as observed at 2θ positions 31.78° (211) along with two other peaks at 32.26° (112) and 32.95° (300) having similar intensities are supportive to ensure the formation Hap as noticed in many other studies (El Khal and Batis 2015; Sultana et al. 2021). This observation is fairly comparable with the standard JCPDS data (File #9-432) (El Khal and Batis 2015; Sultana et al. 2021). However, synthesis of Hap by calcination at high temperature is a well-established method and hitherto quite a significant number of articles (both research and review papers) have published (El Khal and Batis 2015; Refaat et al. 2017; Youness et al. 2017; Naga et al. 2020; Alinavaz et al. 2021). Hence, our interest was to develop Hap without any high-temperature calcination but just using UV-illumination. The XRD diffractogram of the UV-mediated sample (Fig. 3) indexed the distinctive peaks symbolic for Hap and ensured us about becoming successful to reach the target. In addition, this newly developed UV-Hap also appended the peak for β-TCP (tricalcium phosphate) having *d*-spacing values of 2.87 (Å) and 2.60 (Å) together with the peak of calcium carbonate at 2θ position 29.41°. However, for a better understanding on X-ray crystallographic properties of UV-synthesized Hap, our objective was to explore following parameters associated with XRD.

Lattice parameter, crystallite size (D_c), crystallinity degree (X_c), crystallinity index (CI), dislocation density and micro-strain

The first attempt of the crystallographic analysis was concentrated on calculating the lattice parameters using the well-known crystallographic equation for hexagonal system (Murugan and Ramakrishna 2005; Ahmed et al. 2017; Wang et al. 2017). The measured lattice parameters ($a = b = 9.424$ Å, $c = 6.8889$ Å) and the corresponding cell volume ($V = 1587$ Å) for the UV-synthesized Hap were well matched with the JCPDS standard values (File #9-432) (El Khal and Batis 2015; Sultana et al. 2021). This observation indicated that the UV-illumination of the starting materials triggered the Hap formation within fairly right track which is quite promising. However, further supporting information was acquired through a detailed XRD analysis. With the aid of Eqs. 2–6 as described previously (Ahmed et al. 2017), the crystallite size (D_c), crystallinity degree (Xc) and crystallinity index (CI), dislocation density and micro-strain of the UV-Hap were calculated, respectively, and are summarized in Table 1.

$$\text{Crystallite size } D_c = \frac{K_B\,\lambda}{\text{FWHM}\,\cos\theta} \tag{2}$$

where FWHM (Full width at half maxima) is in radian, K_B is the broadening constant equal to 0.9, $\lambda = 1.54$ Å and θ = diffraction angle (in degree).

The well-known Scherrer equation relates to the chosen diffraction peak and many publications considered the sharpest peak to calculate crystallite size (Rabiei et al. 2020). However, in this research work we have chosen the Bragg reflections at three planes, e.g., (211), (112) and (300) to calculate the crystallite size of UV-Hap and an average value was considered which was found to be 83 nm.

$$\text{Crystallinity degree, } X_c = \left(\frac{k_c}{\text{FWHM}}\right)^3 \tag{3}$$

Here, k_c is a constant having the value 0.24 and FWHM is in degree.

Table 1 Crystallographic parameters of UV-Hap and Hap (900 °C)

Hap sample	Crystallinity degree (X_c)	Crystallinity index, CI	Micro-strain, ε	Dislocation density, δ (10^{15} lines/m^2)
UV-Hap	15.92	1.60	0.12	0.16
Hap (900 °C)	15.38	1.54	0.09	0.15

$$\text{Crystallinity index, CI} = \frac{H_{(202)} + H_{(300)} + H_{(112)}}{H_{(211)}} \tag{4}$$

$$\text{Dislocation density, } \delta = \frac{1}{(D_c)^2} \tag{5}$$

$$\text{Micro - strain, } \varepsilon = \frac{\text{FWHM}}{4\tan\theta} \tag{6}$$

where FWHM is in radian and θ = Bragg's angle.

By comparing the data as given in Table 1, it is evident that all the calculated parameters for UV-synthesized Hap satisfied the values observed for calcined Hap. Such results demonstrated the promising synthesis of Hap from eggshell by applying direct UV-illumination.

Biphasic characteristics

Khiri et al. (2019) in their investigation have mentioned that more research need to be deliberated in order to explore the application of the biphasic biomaterial consisting of Hap and β-TCP. We have already discussed that the UV-synthesized Hap resulted in biphasic form where β-TCP was produced as the 2nd phase. Hence, next we proceed for the quantitative analysis of this β-TCP. Following the earlier methods (Ahmed et al. 2017; Saikiran et al. 2020), % and volume fraction of β-TCP is calculated using Eqs. 7–8.

$$\%\beta\text{-TCP} = \frac{I_{\beta\text{-TCP}(0210)}}{I_{\text{Hap}(211)} + I_{\beta\text{-TCP}(0210)}} \tag{7}$$

$$\text{Volume fraction of } \beta\text{-TCP, } X_\beta = \frac{P(\%\beta\text{-TCP})}{1 + (P-1)(\%\beta\text{-TCP})} \tag{8}$$

The coefficient P denotes the integral intensity ratio of hydroxyapatite at (2 1 1) to β-TCP at (0 2 10). The value of P was calculated as 2.275 using the XRD of the mixtures of standard Hap and β-TCP (Ahmed et al. 2017).

It was observed from the analysis that UV-mediated Hap which was formed in biphasic format contains 18.69% β-TCP while volume fraction of β-TCP was 0.343. This observation is quite reasonable since transformation of Hap to β-TCP depends on the sintering temperature (Ahmed et al. 2017; Khiri et al. 2019) and our UV-mediated approach did not use any high temperature.

Assessment of crystallite size using different models

Linear straight line model of Scherrer's equation

The crystallite size of UV-Hap as measured in Sect. 3.2 was further validated using linear straight line model

(LSLM) of Scherrer's equation where all peaks are taken into account to deduce the crystallite size. Comparing with a linear straight line equation, ($y = mx + c$), the Scherrer equation (Eq. 2) can be transformed as:

$$\cos\theta = \frac{K_B\lambda}{D_c} \times \frac{1}{\text{FWHM}} \tag{9}$$

To calculate the crystallite size, a graph as shown in Fig. 4a was plotted where $\frac{1}{\text{FWHM}}$ and cosθ represented the x-axis and y-axis, respectively. The slope of the plot was equal to $\frac{K_B\lambda}{D_c}$ which facilitated the value of D_c to be calculated as 723 nm. Obviously this value is significantly higher than that measured by the simple format of Scherrer equation (Eq. 2).

Similar observation was also discussed in a previous study (Rabiei et al. 2020) where the authors supplemented an explanation on such behavior. They assumed that when the least squares method is applied to fit the data according to the LSLM (Eq. 9) then, certainly the y-intercept does not carry any physical meaning. Hence it indicates that liner straight line model of Scherrer's equation is not applicable for this case (Rabiei et al. 2020) and similar result was observed for Hap synthesized by calcining at 900 °C (Fig. 4b).

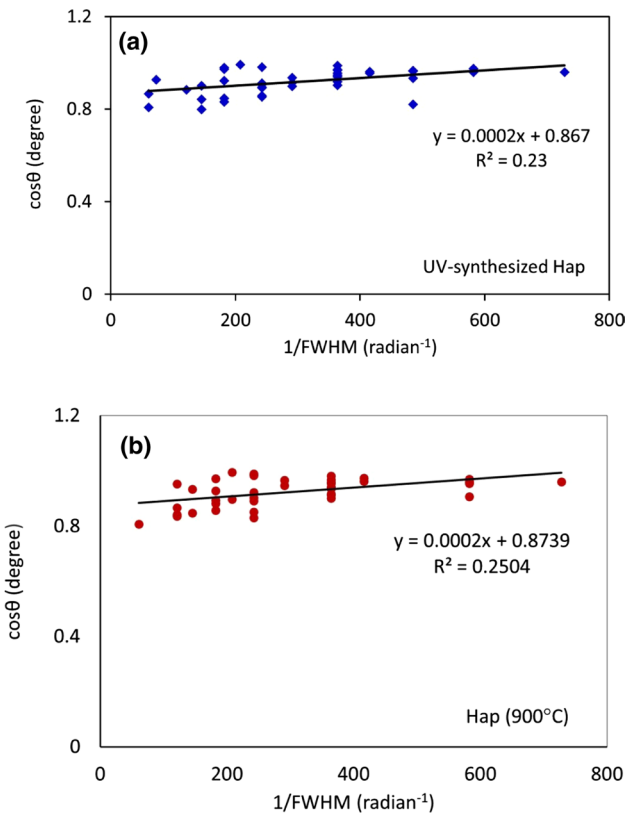

Fig. 4 Validation of crystallite size using liner straight line model of Scherrer equation; **a** UV-Hap; **b** Hap (900 °C)

Model of straight line passing the origin (MSLPO) in Scherrer equation

Next to validate the crystallite size, we applied Model of straight line passing the origin (MSLPO) in Scherrer Equation. In order to complement the lacking of LSLM, a recent study (Rabiei et al. 2020) has developed this model where they purposely forced the linear plot to pass through the origin. Accordingly, the authors considered following Eq. (10) to administer the linear plot to cross the origin giving a rational slope for calculations. Thus they have simplified Eq. (2) as:

$$\cos\theta = \frac{K_B\lambda}{D_c} \times \frac{1}{\text{FWHM}} \tag{10}$$

If cosθ and $\frac{1}{\text{FWHM}}$ represent y and x-axes value, respectively, then slope for the multiple values can be calculated as (Monshi and Messer 1991; Rabiei et al. 2020):

$$\text{Slope} = \frac{x_1y_1 + x_2y_2 + x_3y_3 + x_4y_4 + \cdots\cdots\cdots\cdots\cdots\cdots + x_ny_n}{x_1^2 + x_2^2 + x_3^2 + x_4^2 + \cdots\cdots\cdots\cdots\cdots\cdots\cdots\cdots\cdots\cdots + x_n^2} \tag{11}$$

Applying Eq. (11) we have measured the slope for the case of UV-Hap as 0.002474 and by comparing this slope with that of Eq. 2, the measured crystallite sizes was found to be 56 nm which seemed fairly reasonable.

Monshi–Scherrer model

In order to go for further analysis of the crystallite size of UV-synthesized Hap, we used Monshi–Scherrer model (Monshi and Messer 1991; Rabiei et al. 2020) which is indeed the ln version of Scherrer equation:

$$\ln(\text{FWHM}) = \ln\frac{1}{\cos\theta} + \ln\frac{K_B\lambda}{D_c} \tag{12}$$

The graph ln $\frac{1}{\cos}$ *vs* ln(FWHM) as plotted in Fig. 5a (UV-synthesized Hap) and 5b (Hap at 900 °C) also signifies $y = mx + c$ nature providing the intercept value equal to ln $\frac{K_B\lambda}{D_c}$ which ultimately transformed into following format:

$$\frac{K_B\lambda}{D_c} = e^{\text{intercept}} \tag{13}$$

Monshi–Scherrer model has the advantage of decreasing the errors and thus gives more accurate value of crystallite size (Monshi and Messer 1991; Rabiei et al. 2020). Using Eq. (13), the crystallite size of UV-Hap was obtained as 58 nm. This value is lower than the Liner straight line

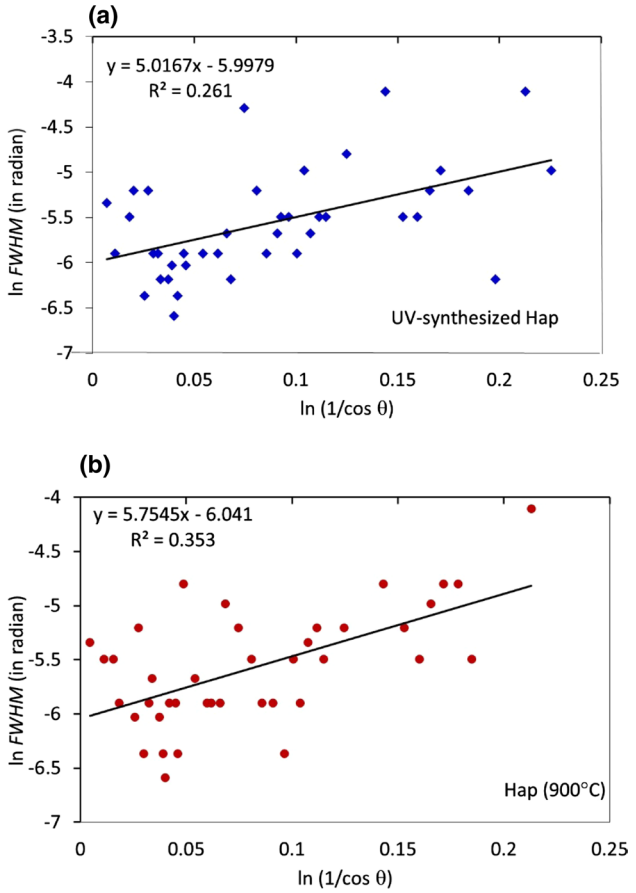

Fig. 5 Validation of crystallite size using Monshi–Scherrer model; **a** UV-Hap; **b** Hap (900 °C)

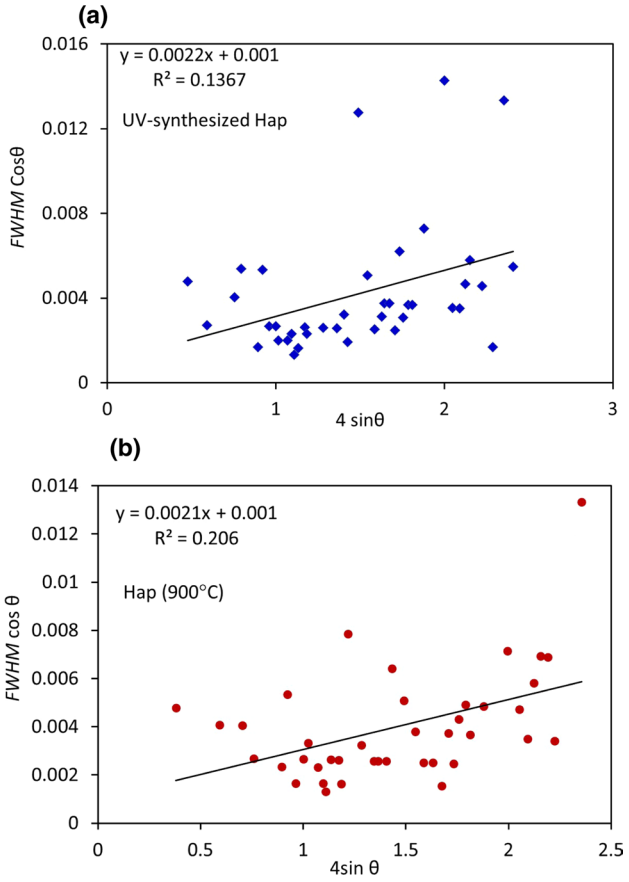

Fig. 6 Validation of crystallite size using Williamson–Hall model; **a** UV-Hap; **b** Hap (900 °C)

model of Scherrer's equation but in agreement with the value obtained using simple Scherrer equation. Thus we concluded that Monshi–Scherrer model is supportive to calculate the crystallite size of UV-Hap and this observation is impartially similar to the earlier result (Rabiei et al. 2020).

Williamson–Hall model

The Scherrer Equation is confined with the effect of crystallite size but not the micro-strain of the lattice. However, Williamson–Hall (W–H) method considers the strain-induced XRD peak broadening and offers the crystal size to be measured along with the intrinsic strain (Rabiei et al. 2020). Conferring to the physical line broadening of X-ray diffraction peak, W–H analysis is expressed as a combination of effect of size and strain:

$$\mathrm{FWHM}_{\mathrm{total}} = \mathrm{FWHM}_{\mathrm{size}} + \mathrm{FWHM}_{\mathrm{strain}} \tag{14}$$

Amalgamation of Eqs. (2), (6) and (14) results Eq. (15):

$$\mathrm{FWHM}_{\mathrm{total}} = \frac{K_{\mathrm{B}}\lambda}{D_{\mathrm{c}}\cos\theta} + 4\varepsilon\ \tan\theta \tag{15}$$

Multiplication of Eq. (15) by cosθ gives the new format as:

$$\mathrm{FWHM}_{\mathrm{total}}\cos = \frac{K_{\mathrm{B}}\lambda}{D_{\mathrm{c}}} + 4\varepsilon\ \sin\theta \tag{16}$$

Equation (16) is known as the W–H Equation which signifies the uniform deformation model (UDM) where the isotropic state of the crystal is presumed and the strain uniformity in all directions is taken into account. Nevertheless, a plot of 4sinθ (x-axis) vs $\mathrm{FWHM}_{\mathrm{total}}$ cosθ (y-axis) facilitated the linear fit of the data and the crystallite size of UV-Hap (Fig. 6a) and calcined Hap (Fig. 6b) was estimated as 138 nm from the y-intercepts. Again it is clearly visualized that this value is higher than that found from Scherrer equation (Eq. 2). Since, the values of $\mathrm{FWHM}_{\mathrm{strain}}$ and ε were rather calculated but not directly obtained from XRD data, hence this could be the plausible reason for such discrepancy (El-Sadek et al. 2019; Nath et al. 2020).

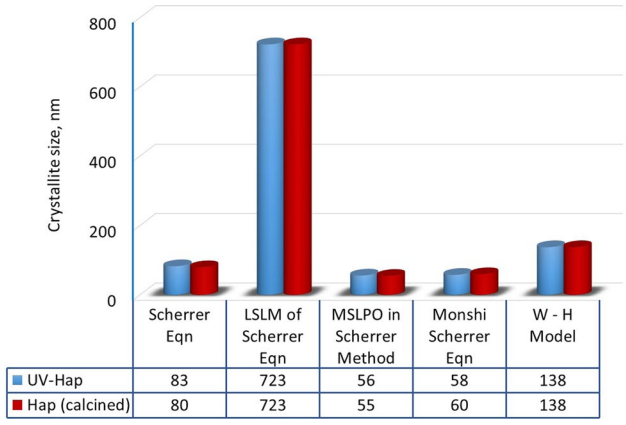

Fig. 7 Summary of calculated crystallite size obtained from different models

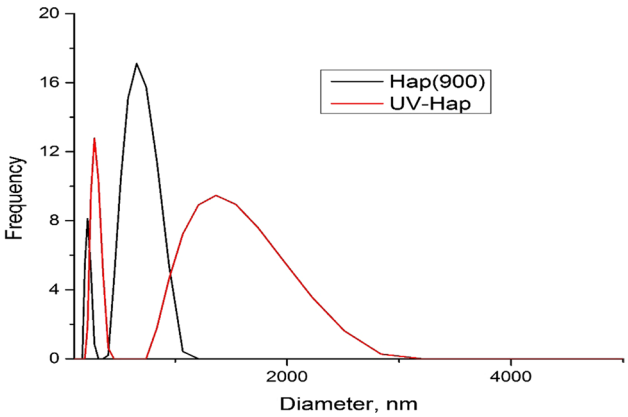

Fig. 8 Particle size distribution of UV-Hap and Hap (900 °C)

Nevertheless, to compare all the crystallite size values of UV-Hap as obtained from the above equations we discussed, were compared with the calculated crystallite size of Hap synthesized at 900 °C and summarized as a bar chart (Fig. 7). Interestingly, the crystallite sizes of both Hap samples as measured by (1) Scherrer equation; (2) MSLPO in Scherrer method; and (3) Monshi–Scherrer equation are < 100 nm which indicates that these three models are fairly suitable in calculating the crystallite size. On the other hand, LSLM of Scherrer equation and W–H models gives the crystallite size values 723 nm and 138 nm, respectively, indicating that these two models are not appropriate to measure the crystallite size of UV-Hap.

Particle size analysis

Though in this paper we intended to explore the XRD analysis of the UV-synthesized Hap but additionally we have also focused on particle size analysis. Given in Fig. 8 represents the particle size distribution of UV-Hap and the calcined Hap.

A bimodal type particle size distribution is observed where for the first distribution the average particle diameter was 303 nm and 310 nm for calcined Hap and UV-Hap, respectively. On the other hand, these values were extremely in the upward direction for the second distribution (721 nm for calcined Hap and 896 nm for UV-Hap). The larger particles in DLS measurement possibly be linked to the agglomeration of the particles which is quite usual. This agglomeration nature is also supported by the measured zeta potential values. Observed zeta potential values for UV-Hap and calcined Hap were found to be 3.9 and 4.1 mV. Since, these values are below ± 10 mV, the particles possess a strong tendency to agglomerate (Oberbek et al. 2018).

Conclusion

Applying UV-radiation to the eggshell powder, Hap has been synthesized successfully and its crystallographic characteristics were assessed by employing XRD. In particular crystallite size of this newly developed UV-sensitized Hap was measured and compared using different well-known equations, e.g., Scherrer equation, Model of straight line passing the origin (MSLPO) in Scherrer Equation, Monshi–Scherrer model, Liner straight line model (LSLM) of Scherrer's Equation and Williamson–Hall (W–H) model. Among these five models, first three models appeared as accurate by facilitating reasonable crystallite size values which were < 100 nm. But the later two models, i.e., LSLM of Scherrer's equation and W–H model were inaccurate for the synthesized Hap as the crystallite size were above the nanoscale of 100 nm. However, all the parameters analyzed in this work to characterize UV-mediated Hap were in good agreement with the Hap synthesized by customary solid state calcination method. Such results are fairly informative to establish the UV-illumination method as a promising alternative to synthesis Hap at ambient temperature and this is the novelty of this research work.

Acknowledgments The authors are grateful to Bangladesh Council of Scientific and Industrial Research (BCSIR) authority for financial support through R&D project (ref. no. 39.02.0000.011.14.134.2021/900; Date: 30.12.2021). Thanks to the Central Analytical Research Facilities (CARF), BCSIR for DLS particle size analysis.

Declarations

Conflict of interest The authors declare that they have no competing interests.

References

Ahmed S, Nigar F, Mustafa AI, Ahsan M (2017) Dopant ion concentration and calcination temperature dependent crystallographic behaviour of fluoride and iron doped hydroxyapatite. Trans Indian Ceram Soc 76:215–221

Alinavaz S, Mahdavinia GR, Jafari H et al (2021) Hydroxyapatite (HA)-based hybrid bionanocomposite hydrogels: ciprofloxacin delivery, release kinetics and antibacterial activity. J Mol Struct 1225:129095

Anderson W, Kozak D, Coleman VA et al (2013) A comparative study of submicron particle sizing platforms: accuracy, precision and resolution analysis of polydisperse particle size distributions. J Colloid Interface Sci 405:322–330

Becerra J, Rodriguez M, Leal D et al (2022) Chitosan-collagen-hydroxyapatite membranes for tissue engineering. Springer. https://doi.org/10.1007/s10856-022-06643-w. Accessed 18 Jul 2022

Coelho CC, Grenho L, Gomes PS et al (2019) Nano-hydroxyapatite in oral care cosmetics: characterization and cytotoxicity assessment. Sci Rep 9:1–10

El Khal H, Batis NH (2015) Effects of temperature on the preparation and characteristics of hydroxyapatite and its adsorptive properties toward lead. New J Chem 39:3597–3607

El-Sadek A, Wasly HS, Batoo KM (2019) X-ray peak profile analysis and optical properties of CdS nanoparticles synthesized via the hydrothermal method. Appl Phys A 125:1–17

Gallinetti S, Canal C, Ginebra M-P (2014) Development and characterization of biphasic hydroxyapatite/β-TCP cements. J Am Ceram Soc 97:1065–1073

Hossain MS, Shaikh MAA, Rahaman MS, Ahmed S (2022) Modification of the crystallographic parameters in a biomaterial employing a series of gamma radiation doses. Mol Syst Des Eng. https://doi.org/10.1039/D2ME00061J

Huixia L, Yong L, Yanni T et al (2015) Room temperature gas sensing properties of tubular hydroxyapatite. New J Chem 39:3865–3874

In Y, Amornkitbamrung U, Hong M-H, Shin H (2020) On the crystallization of hydroxyapatite under hydrothermal conditions: role of sebacic acid as an additive. ACS Omega 5:27204–27210. https://doi.org/10.1021/acsomega.0c03297

Khiri MZA, Matori KA, Zaid MHM et al (2019) Crystallization behavior of low-cost biphasic hydroxyapatite/β-tricalcium phosphate ceramic at high sintering temperatures derived from high potential calcium waste sources. Results Phys 12:638–644

Maleki B, Chahkandi M, Tayebee R et al (2019) Synthesis and characterization of nanocrystalline hydroxyapatite and its catalytic behavior towards synthesis of 3,4-disubstituted isoxazole-5 (4H)-ones in water. Appl Organomet Chem 33:e5118

Monshi A, Messer PF (1991) Ratio of slopes method for quantitative X-ray diffraction analysis. J Mater Sci 26:3623–3627

Murugan R, Ramakrishna S (2005) Crystallographic study of hydroxyapatite bioceramics derived from various sources. Cryst Growth Des 5:111–112

Naga SM, Hassan AM, Awaad M et al (2020) Forsterite/nano-biogenic hydroxyapatite composites for biomedical applications. J Asian Ceram Soc 8:373–386

Nasiri S, Hosseinnezhad M, Rabiei M et al (2021) The effect of calcination temperature on the photophysical and mechanical properties of copper iodide (5 mol%)–doped hydroxyapatite. Opt Mater 121:111559

Nath D, Singh F, Das R (2020) X-ray diffraction analysis by Williamson–Hall, Halder–Wagner and size-strain plot methods of CdSe nanoparticles—a comparative study. Mater Chem Phys 239:122021

Oberbek P, Bolek T, Chlanda A et al (2018) Characterization and influence of hydroxyapatite nanopowders on living cells. Beilstein J Nanotechnol 9:3079–3094

Ooi C-H, Ling YP, Abdullah WZ et al (2019) Physicochemical evaluation and in vitro hemocompatibility study on nanoporous hydroxyapatite. J Mater Sci Mater Med 30:44. https://doi.org/10.1007/s10856-019-6247-5

Rabiei M, Palevicius A, Monshi A et al (2020) Comparing methods for calculating nano crystal size of natural hydroxyapatite using X-ray diffraction. Nanomaterials 10:1627

Rabiei M, Palevicius A, Dashti A et al (2021a) X-ray diffraction analysis and Williamson–Hall method in USDM model for estimating more accurate values of stress–strain of unit cell and super cells ($2 \times 2 \times 2$) of hydroxyapatite, confirmed by ultrasonic pulse-echo test. Materials 14:2949

Rabiei M, Palevicius A, Ebrahimi-Kahrizsangi R et al (2021b) New approach for preparing in vitro bioactive scaffold consisted of ag-doped hydroxyapatite+ polyvinyltrimethoxysilane. Polymers 13:1695

Refaat A, Youness RA, Taha MA, Ibrahim M (2017) Effect of zinc oxide on the electronic properties of carbonated hydroxyapatite. J Mol Struct 1147:148–154

Saikiran A, Vivekanand M, Prahalad M et al (2020) Microwave synthesis of Zn/Mg substituted and Zn/Mg-F co-substituted nanocrystalline hydroxyapatite. Mater Today Proc 27:2355–2359

Sharifi S, Lotfipour F, Ghavimi MA et al (2021) Hydroxyapatite-gelatin and calcium carbonate-gelatin nanocomposite scaffolds: Production, physicochemical characterization and comparison of their bioactivity in simulated body fluid. Eurasian Chem Commun 3:70–80

Sultana S, Hossain MS, Mahmud M et al (2021) UV-assisted synthesis of hydroxyapatite from eggshells at ambient temperature: cytotoxicity, drug delivery and bioactivity. RSC Adv 11:3686–3694

Wang H, Yuan L, An J (2017) Crystallographic characteristics of hydroxylapatite in hard tissues of cololabis saira. Curr Comput Aided Drug Des 7:103

Youness RA, Taha MA, Ibrahim MA (2017) Effect of sintering temperatures on the in vitro bioactivity, molecular structure and mechanical properties of titanium/carbonated hydroxyapatite nanobiocomposites. J Mol Struct 1150:188–195